

Phase locking of equatorial Atlantic variability through the seasonal migration of the ITCZ

INGO RICHTER

Application Laboratory, JAMSTEC, Yokohama Japan

SHANG-PING XIE

Scripps Institution of Oceanography, University of California at San Diego, La Jolla, California, USA

YUSHI MORIOKA, TAKESHI DOI, BUNMEI TAGUCHI¹, AND SWADHIN BEHERA

Application Laboratory, JAMSTEC, Yokohama Japan

¹ current affiliation: *Research Center for Advanced Science and Technology, University of Tokyo, Japan*

Climate Dynamics

submitted, 23 October 2015

revised, 15 February 2016

revised, 6 June 2016

accepted, 19 July 2016

Corresponding author address:

Ingo Richter

Application Laboratory, JAMSTEC, 3173-25 Showa-machi, Kanazawa-ku, Yokohama, Kanagawa 236-0001, Japan

E-mail: richter@jamstec.go.jp

ABSTRACT

The equatorial Atlantic is marked by significant interannual variability in sea-surface temperature (SST) that is phase-locked to late boreal spring and early summer. The role of the atmosphere in this phase locking is examined using observations, reanalysis data, and model output. The results show that equatorial zonal surface wind anomalies, which are a main driver of warm and cold events, typically start decreasing in June, despite SST and sea-level pressure gradient anomalies being at their peak during this month. This behavior is explained by the seasonal northward migration of the intertropical convergence zone (ITCZ) in early summer. The north-equatorial position of the Atlantic ITCZ contributes to the decay of wind anomalies in three ways: 1) Horizontal advection associated with the cross-equatorial winds transports air masses of comparatively low zonal momentum anomalies from the southeast toward the equator. 2) The absence of deep convection leads to changes in vertical momentum transport that reduce the equatorial wind anomalies at the surface, while anomalies aloft remain relatively strong. 3) The cross-equatorial flow is associated with increased total wind speed, which increases surface drag and deposit of momentum into the ocean.

Previous studies have shown that convection enhances the surface wind response to SST anomalies. The present study indicates that convection also amplifies the surface zonal wind response to sea-level pressure gradients in the western equatorial Atlantic, where SST anomalies are small. This introduces a new element into coupled air-sea interaction of the tropical Atlantic.

1. Introduction

Sea-surface temperature (SST) in the equatorial Atlantic is subject to interannual variability that has significant impacts on the surrounding continents (Folland et al. 1986; Nobre and Shukla 1996). SST anomalies occur along the equatorial wave-guide with the maximum amplitude of about 1K occurring in the eastern cold tongue region. This mode of variability is often called the Atlantic Zonal Mode (AZM) due to its zonal orientation. The AZM is considered to rely on mechanisms similar to El Niño/Southern Oscillation (ENSO) as highlighted by Zebiak (1993). Due to this apparent similarity warm and cold events are also sometimes called Atlantic Niños and Atlantic Niñas, respectively. Compared to ENSO, however, the AZM is shorter lived (3 months versus 9 months), its amplitude is weaker (1K vs. 3K), and its peak is phase-locked to boreal summer (JJA), as opposed to boreal winter (DJF) in the case of ENSO.

While our understanding of the AZM has increased over the years (Zebiak 1993; Carton 1994; Xie and Carton 2004; Chang et al. 2006; Keenlyside and Latif 2007), recent results indicate that the analogy with ENSO may not carry as far as previously thought. Foltz and McPhaden (2010), Lübbecke and McPhaden (2012), and Richter et al. (2013) show that off-equatorial influences play an important role in some AZM events, while Richter et al. (2014b) present evidence that coupled air-sea feedbacks are weaker than suggested by previous studies. Furthermore, the representation of the equatorial Atlantic in general circulation models (GCMs) is notoriously difficult and has been a longstanding problem (Davey et al. 2002; Richter and Xie 2008; Richter et al. 2014a). Models typically overestimate SST in the eastern cold tongue region, while underestimating them in the west, leading to a zonal SST gradient whose sign is opposite to observations. The persistent mean state biases in GCMs likely contribute to the models' misrepresentation of the AZM (Breugem et al. 2006; Richter et al. 2014a) and the poor prediction skill of dynamical models for the region, which is often on a level with persistence forecasts (Stockdale et al. 2006). The limited applicability of the ENSO mechanism to the AZM as well as the poor prediction skill for AZM events indicate that a more complete understanding of the phenomenon is needed. One important issue is to understand why the AZM is tightly locked to the annual cycle. This involves two questions: 1) why do events typically develop in boreal spring, and 2) why do events terminate after just three months in boreal summer?

Keenlyside and Latif (2007; KL07 hereafter) explain the phase locking of the AZM in terms of the seasonality of coupled feedbacks. They show that the zonal surface winds in the western equatorial Atlantic are most sensitive to eastern equatorial Atlantic SST anomalies in late spring and early summer. KL07 attribute this to the mean state SST in the western equatorial Atlantic, which only during those months rises above 28°C and thus permits deep convection. The implicit assumption is that the presence of deep convection will enhance the response to SST anomalies through diabatic latent heating as moisture condenses in convective updrafts in the atmosphere. The importance of the seasonal cycle in limiting the length of AZM events is also shown by Bates (2008, 2010) who conducts anomaly-coupled GCM sensitivity experiments with a fixed mean state and insolation representative of the annual mean or individual seasons. She finds that the length of AZM events roughly triples with a perpetual annual mean basic state, and that AZM variability is enhanced with perpetual boreal spring or fall conditions. Bates also suggests that the position of the ITCZ, through its influence on the strength of the climatological trade winds, plays an important role in this. While both KL07 and Bates (2008, 2010) stress the role of the ITCZ in equatorial wind anomalies the detailed mechanism awaits further investigation.

The importance of diabatic heating in modulating the surface wind response to interannual SST anomalies has long been recognized. Webster (1981) investigated the atmospheric response to SST anomalies in a simple model with a convergence-heating feedback that allowed convective heating to modify surface convergence until equilibrium was reached. Zebiak (1986) additionally considered the importance of the background state by allowing heating in a given location to occur only if the sum of the (predicted) anomalous and (prescribed) climatological wind fields was convergent there. This hypothesized influence of the background state on the convergence feedback has also been invoked to explain the phase locking of ENSO to boreal winter (Harrison and Vecchi 1999; Vecchi 2006). Focusing on the 1997/98 event, the authors showed that the climatological strengthening of the South Pacific Convergence Zone (SPCZ) in December was associated with a southward shift of equatorial westerly wind anomalies toward the region of maximum SST and precipitation. This led to strengthening easterlies on the equator that, through oceanic Kelvin waves, terminated the El Niño event in subsequent months. McGregor et al. (2012) used an intermediate complexity model to investigate the southward shift of ENSO zonal wind anomalies

in more detail and argued that it is related to the seasonal reduction of wind speed that accompanies the southward shift of convection. This, they suggested, leads to reduced damping of surface momentum, which strengthens Ekman pumping and allows inter-annual surface wind anomalies to intensify south of the equator.

The above ENSO studies rely on the same basic argument as KL07 to explain seasonal phase locking, namely that the seasonal migration of maximum SST and precipitation away from the equator is responsible for the decay of equatorial wind anomalies, which eventually leads to the termination of events. In the present study we expand on the results of KL07 and examine in more detail the relation between deep convection and surface wind variability in the equatorial Atlantic. Furthermore, we examine what commonalities, in terms of phase locking, exist among the equatorial Atlantic, Pacific and Indian Ocean basins. The rest of the paper is structured as follows. In section 2 we introduce the data sets used in this study. In section 3 we review the climate of the tropical Atlantic and highlight some crucial aspects of the AZM. This is followed by a detailed examination of AZM phase locking (section 4) and a comparison with other basins (section 5). In section 6, we summarize our results and discuss their ramifications.

2. Data and methods

The emphasis of this study lies on observational and reanalysis data for the period 1982-2013. The choice of this period was motivated by the fact that it falls into the satellite observation era, which offers good coverage of precipitation and surface winds over the ocean. Precipitation is from the Global Precipitation Climatology Project (GPCP) version 2.2, which is a blend of satellite and station data (Adler et al. 2003). Surface winds are from the European Centre for Medium Range Weather Forecasts (ECMWF) Interim reanalysis (ERA-Interim hereafter; Dee et al. 2011). The surface winds of the ERA-Interim match well with those from satellite products for the period 1986-2013 but extend further back and were therefore chosen for our analysis period. For SST we use the Optimally Interpolated SST (OISST) dataset of Reynolds et al. (2002), which is a blend of satellite, ship-based, and buoy observations. For oceanic subsurface temperatures we rely on the ECMWF ocean reanalysis (ORAS4; Balmaseda et al. 2013). The forcing of ORAS4 is based on the ERA-Interim surface winds and thus provides consistency between the two reanalyses.

We supplement our analysis with several GCM simulations from the Coupled Model Intercomparison Project Phase 5 (CMIP5), which offer the advantage of physically consistent and gap-free data. The experiment considered here is the Atmospheric Model Intercomparison Project (AMIP), in which atmospheric GCMs (AGCMs) are run with SSTs prescribed from observations for the period 1979-2008. Most coupled ocean-atmosphere GCMs in CMIP5 suffer from severe SST biases in the tropical Atlantic and do not achieve a realistic representation of the AZM (Richter et al. 2014a). Using AMIP runs has the advantage of avoiding these unrealistic SST distributions and allows to average over a model ensemble (see Table 1 for ensemble members) because the SST forcing is the same in all models.

Several indices are used in our analysis (see Fig. 1b for a geographical illustration). The ATL3 (originally defined by Zebiak [1993] in analogy to the Pacific Niño 3 index) captures SST variability in the cold tongue region ($20^{\circ}\text{W}-0, 3^{\circ}\text{S}-3^{\circ}\text{N}$) and is a standard indicator of the AZM. The western equatorial wind index (WEA; $40-20^{\circ}\text{W}, 2^{\circ}\text{S}-2^{\circ}\text{N}$) covers the area of maximum zonal surface wind variability in the equatorial Atlantic and a similarly defined index has been used in other studies (e.g. KL07).

We use composite analysis to examine the evolution of AZM events. For the observations we composite the years 1988, 1991, 1995, 1996, 1999, and 2008 because they represent canonical Atlantic Niño events that resemble ENSO dynamics. The years 1987, 1998, and 2006 also featured warm anomalies in the ATL3 but were not chosen because their evolution follows a different pattern (Richter et al. 2013). Similarly, we picked 1982, 1983, 1992, 1994, 1997, and 2005 to composite canonical cold AZM events.

Finally, we note that we use the term “anomaly” exclusively to mean departure from the long-term monthly mean (i.e. interannual variations) rather than departure of the seasonal cycle from the annual mean. For the current analysis we did not attempt to remove the climate change signal through linear detrending because the analysis period is rather short and subject to significant decadal variability.

3. Tropical Atlantic mean climate and its interannual variability

The climate of the tropical Atlantic is marked by persistent northeasterly and southeasterly trade winds (Fig. 1) that typically converge close to the equator where they fuel intense precipitation in the intertropical convergence zone (ITCZ). While the trade winds blow fairly steadily, the location of their convergence varies by season.

This is reflected in the position of the ITCZ, which reaches its southernmost latitude in boreal spring (MAM; Fig. 1a) and its northernmost latitude in boreal summer (JJA; Fig. 1b). The northward migration of the ITCZ is linked to the annual cycle of insolation, which warms both SST and land surface temperatures north of the equator (Xie and Carton 2004; Chang et al. 2006; KL07), though the relative importance of oceanic and continental influences remains under debate (Biasutti et al. 2003, 2005; Okumura and Xie 2004). The latitudinal shift of the ITCZ from the equator in MAM to about 8°N in JJA is accompanied by intensification of the equatorial easterlies as the southeast trades flow across the equator and into the ITCZ (Fig. 1). The intensification is most pronounced over the western equatorial Atlantic, where the near-surface easterlies strengthen from 3.2 m/s in April to 5.4 m/s in July, based on ERAI data averaged over the WEA index (see section 2 for index definitions). Through the excitation of equatorial Kelvin waves, the strengthened easterlies shoal the eastern equatorial Atlantic thermocline, which facilitates upwelling-related cooling and the formation of the Atlantic cold tongue (Fig. 1b). In the ATL3 region, SSTs drop from 28.8°C in April to 24.6°C in July.

The timing and magnitude of the surface wind intensification on the equator varies considerably from year to year and this leads to interannual SST variability in the cold tongue region where the AZM attains maximum amplitude. Some studies suggest that the AZM relies on the following positive coupled air-sea feedback mechanism (Philander 1986; Zebiak 1993; KL07, Ding et al. 2010): 1) an initial surface wind anomaly on the equator leads to thermocline readjustment through Kelvin waves; 2) the resulting thermocline changes generate SST anomalies in the eastern equatorial Atlantic through upwelling; 3) the SST anomalies alter the zonal pressure gradient along the equator in such a way as to reinforce the initial wind anomaly. This coupled feedback mechanism is often referred to as the Bjerknes feedback and has been shown to be an important component of equatorial Pacific variability (Bjerknes 1969; Chang et al. 2006).

Figure 2 shows the composite evolution of an AZM warm event based on the ORAS-4 ocean reanalysis. All indices are normalized by their respective standard deviations. Westerly wind stress anomalies in the WEA region exceed 0.5 standard deviations (SD) from March, peak in May, and decay rapidly thereafter. The depth of the 20°C isotherm (Z20 hereafter) in the ATL3 region follows with some lag, with

values exceeding 0.5 SD in May and reaching their peak in June. The evolution of SST anomalies in the ATL3 region follows that of Z20 but decays more gradually.

If one takes the Atlantic Bjerknes feedback as given it is clear that there needs to exist a process that breaks the positive feedback loop or else the AZM would remain in its positive state indefinitely. Ocean dynamics may contribute to this but here we focus on the role of the atmosphere. In this context it is interesting to note that during the peak of the SST anomalies in June the wind anomalies have already decreased by about 50% relative to their maximum in May. In the following section we examine this behavior in more detail.

4. Phase locking of the Atlantic zonal mode

4.1. Composite analysis

We start by analyzing the evolution of composite warm events in observations (Fig. 3). SST anomalies in the central equatorial Atlantic start developing in March, peak in June, and decay in July and August. We note that significant SST anomalies also occur along the western coast of southern Africa. Some studies consider these two areas to be part of the same mode of variability (e.g. Huang et al. 2004; Huang and Shukla 2005; Lübbecke et al. 2010) and they may be linked via large-scale anomalies in the position and strength of the subtropical anticyclone (Lübbecke et al. 2010; Richter et al. 2010). Here, however, we focus on equatorial Atlantic winds and the ITCZ and leave aside the linkage to the subtropics.

The close correspondence between surface wind anomalies and ITCZ position is evident in Fig. 3. Both surface wind anomalies and ITCZ are roughly centered on the equator in March and April. As the ITCZ starts shifting northward in May and June the surface wind anomalies do likewise. This leads to weaker anomalies on the equator in June. As the ITCZ firmly establishes itself north of the equator in July and August, westerly wind anomalies remain strong there. On the equator, however, wind anomalies completely cease, while SST anomalies start decaying.

We zoom into the equatorial Atlantic and contrast the composite pressure and wind anomalies at the surface (Fig. 4a) with geopotential height and wind anomalies at 700 hPa (Z700; Fig. 4b). This shows that, unlike the surface wind anomalies, the 700 hPa wind anomalies are rather symmetric about the equator and indifferent to the position of the Atlantic ITCZ. Accordingly, the 700 hPa wind anomalies remain strong in June and July, when the ITCZ moves north of the equator. This is explained

by the fact that precipitation anomalies stay closer to the equator than the ITCZ (Fig. 4b). Nevertheless, it is evident that precipitation anomalies, too, shift westward and off the equator as the cold tongue develops in the eastern equatorial Atlantic (Fig. 1), which suggests that the cool SSTs inhibit convective anomalies.

Both SLP and Z700 anomalies show a large-scale east-west gradient not only on the equator but also in the subtropics. The equatorial Z700 gradient remains prominent until July and, consistently, the anomalies at 700 hPa remain westerly. The large-scale Z700 gradient on the equator is likely influenced by the anomalous SST and convection there. It is not clear, however, whether the negative Z700 anomalies over West Africa and the subtropical South Atlantic are directly linked to the equatorial convection anomalies. We conclude that large-scale influences likely contribute to the westerly wind anomalies at 700 hPa but that the presence of the Atlantic ITCZ is needed for these anomalies to be expressed at the surface.

The evolution of cold AZM events follows a very similar pattern (Fig. 5). While the sign of anomalies is reversed, the seasonal migration of the ITCZ proceeds in a very similar fashion and is accompanied by a weakening of surface wind anomalies on the equator. As in warm events, the maximum surface wind anomalies shift northward with the position of the ITCZ while roughly retaining their orientation. An interesting difference is that the SST anomalies extend all the way to the coast during negative events but are focused in the central basin during positive events. This may be due to differences in the total wind field: during negative events the total winds in the eastern equatorial Atlantic become upwelling favorable and produce a response all the way to the eastern boundary.

4.2. Testing the convergence feedback

Zebiak (1986) argued that the surface wind response to SST anomalies should be enhanced in the presence of deep convection because the associated convective heating enhances the sea-level pressure anomalies. Thus the zonal wind response to ATL3 SST anomalies should be enhanced when deep convection occurs there (see schematic in Fig. 10). Assuming a Matsuno-Gill pattern (Matsuno 1996, Gill 1980), the strongest wind response to this anomalous convection is expected over the western equatorial Atlantic (e.g. Jin 1997, Neelin et al. 1998).

We would like to test to what extent the idealized concept of the convergence feedback matches observations. We do this by sorting monthly fields into two groups

according to GPCP total precipitation in the ATL3. Group one contains months with ATL3 precipitation less than 1 mm/day, and group 2 contains the remaining months. For both groups we regress WEA zonal surface wind on ATL3 SST and compare the results. For the first group, with ATL3 precipitation below 1 mm/day, we find a regression coefficient of $0.54 \text{ m s}^{-1} \text{ K}^{-1}$ (not shown). As expected, the regression coefficient is higher in the second group, with $0.86 \text{ m s}^{-1} \text{ K}^{-1}$, corresponding to a 59% increase over group 1. These results are roughly consistent with those from the simple parameterization in Zebiak (1986). The correlation coefficient, however, is relatively low for both groups (0.56 and 0.50 for groups 1 and 2, respectively) indicating that ATL3 SST anomalies explain only a modest fraction of WEA surface wind variability. This may partly be due to the anomalous precipitation maximum being located to the west of the ATL3 region (Fig. 4b). It may also be argued that, due to this mismatch, the ATL3 and WEA indices are not ideally suited for exploring the convergence feedback. We have therefore repeated the calculation for different index regions but found the results to be qualitatively robust.

The relatively weak link between ATL3 SST anomalies and WEA winds motivates us to also inspect the influence of convection in the WEA region itself (left hand side of schematic Fig. 10). Assuming a Matsuno-Gill response, heating centered on the WEA region should induce wind anomalies of opposite sign to the east and west. Since these partially cancel we expect the direct wind response in the WEA to be relatively small (this is, of course, based on very idealized assumptions; the real wind response will be more complicated due to the zonally elongated heating anomaly, among other things). Nevertheless, we would like to investigate whether convection in the WEA can somehow modulate the surface wind response to remotely induced surface pressure gradients. We therefore use the above binning method but average precipitation over the WEA rather than ATL3 region and set 2 mm/day as the binning criterion. Based on the two bins thus defined, we regress WEA surface zonal wind anomalies on WEA zonal SLP gradient anomalies in the observations (Figs. 6a and 6b). (The SLP gradient is calculated for all relevant grid cells first and then area-averaged.) For the months with WEA precipitation less than 2 mm/day, the analysis yields a correlation coefficient of 0.76 and a regression coefficient of $3.15 \cdot 10^4 \text{ m}^3 \text{ s kg}^{-1}$. For the months with WEA precipitation greater than 2 mm/d the values are 0.77 and $5.30 \cdot 10^4 \text{ m}^3 \text{ s kg}^{-1}$, respectively. Thus the surface zonal wind is 68% more sensitive to zonal pressure gradients when deep convection is present. The convergence

feedback cannot explain this behavior because it only concerns the pressure response to a given SST anomaly. Put differently, the convergence feedback amplifies the SLP response to a given SST anomaly ($\partial SLP'/\partial SST'$) when deep convection is present; it should not alter the sensitivity of surface zonal winds to SLP gradients ($\partial U'/\partial SLP'$). Our results therefore suggest that the convergence feedback cannot fully explain the strong influence of deep convection on the surface wind response to SST anomalies.

We also subject the variability of the AMIP ensemble mean to the same analysis. Here the correlation coefficients are substantially higher (0.87 and 0.90 for low and high precipitation months, respectively), partly because atmospheric noise is averaged out. The regression coefficients are $2.15 \cdot 10^4 \text{ m}^3 \text{ s kg}^{-1}$ and $5.05 \cdot 10^4 \text{ m}^3 \text{ s kg}^{-1}$ for low and high precipitation months, respectively. This indicates that the surface wind sensitivity to the zonal pressure gradient increases by about 130%, significantly more than in the observations.

4.3. Analysis of the surface momentum budget

The above results indicate that the convergence feedback cannot fully explain the increased sensitivity of surface winds to SST anomalies in the presence of convection, which is crucial to the phase-locked nature of equatorial surface wind anomalies. To further examine the reason for the rapid decay of surface zonal wind anomalies in June, we turn to a budget analysis of the surface zonal momentum in the WEA region using ERAI reanalysis data (Fig. 7). The equation forming the basis of this analysis is

$$\frac{\partial u}{\partial t} + u \frac{\partial u}{\partial x} + v \frac{\partial u}{\partial y} - f v + \frac{1}{\rho} \frac{\partial p}{\partial x} + \tau_x = R$$

where τ_x is the surface zonal wind stress (with the sign opposite to that of the surface zonal wind to indicate loss of atmospheric momentum to the ocean), R is the residual of all the other terms on the left-hand side, and the other symbols have their conventional meaning. Transients are neglected in this analysis because they have been shown to give only minor contributions in a similar analysis of Richter et al. (2014b). Vertical momentum transport is difficult to estimate in this simple off-line analysis because parameterized terms, such as entrainment into the atmospheric boundary layer (ABL), are not available and vertical velocity is highly uncertain. We therefore estimate vertical transport as the residual of the budget, denoted by R , multiplied by -1 to show the term that would be needed to close the budget. The Coriolis term is calculated but not plotted because it is negligible on the equator.

The budget analysis reveals that the pressure gradient term has its highest (west-erly) value in June (Fig. 7), which coincides with the peak in the ATL3 SST anomaly. This response of the pressure gradient to SST anomalies is consistent with the simple model of Lindzen and Nigam (1987). The surface winds, however, do not follow a Lindzen-Nigam response but rather decrease in June (Fig. 2). This is due to several factors to be discussed in the following. 1) Horizontal advection contributes to the decrease of surface zonal winds with approximately -0.5 m/s/day. Both zonal and meridional advection (not shown) contribute to this because the mean cross-equatorial south-easterlies in JJA (Fig. 1b) advect relatively weak wind anomalies (Fig. 3) to the equator. 2) Surface wind stress removes momentum from the atmosphere and injects it into the ocean. The standard bulk formula for surface wind stress is $\tau_x = C_D \rho \|\vec{U}\| u$, where C_D is the drag coefficient, ρ is surface air density, $\|\vec{U}\|$ is the surface wind speed, and u is the zonal component of the surface wind. The formula suggests that surface zonal stress roughly follows surface zonal wind. The dependence on surface wind speed, however, introduces a non-linearity, which turns out to be significant. As the total wind speed on the equator increases in JJA (Fig. 8), the same surface zonal wind anomaly will induce greater surface zonal stress. Thus the surface zonal stress decreases less rapidly than the zonal surface wind itself. This is evident in the composite evolution of anomalous zonal wind stress and surface wind (Fig. 8). After the peak in May, the anomalous surface zonal wind decreases appreciably faster than the anomalous zonal wind stress. The product of climatological wind speed and zonal surface wind anomaly, on the other hand, tracks the anomalous zonal wind stress fairly well. 3) Vertical momentum transport (as estimated from the residual) contributes -0.6 m/s/day. A possible interpretation is that, as deep convection moves away from the equator, ABL entrainment intensifies and transports easterly momentum from the lower troposphere into the ABL, thus opposing the westerly wind anomaly. It is difficult to ascertain, however, if this hypothesis has any merit because the vertical structure of the lower troposphere is not well observed over the equatorial Atlantic and thus there is little constraint on the reanalysis. For what it is worth, the ERAI data do suggest that the vertical distribution of momentum in the lower troposphere is more uniform in June and July than in April and May, as shown in the time-pressure section of total zonal wind averaged over the WEA region (Fig. 9). While the total zonal wind in boreal summer is increasing between 1000 and 900 hPa, it is decreasing between

850 and 700 hPa, which is consistent with entrainment of momentum from those upper levels into the ABL.

The time-pressure section (Fig. 9) also reveals that the maximum zonal wind anomaly over the WEA region occurs in May at about 925 hPa. From June through August this maximum somewhat weakens and shifts upward to the 700 hPa level. During the same period, the surface wind anomalies decrease rapidly, leading to a strong vertical shear in the anomalous zonal wind. This is consistent with the composite evolutions at the surface and 700 hPa shown in Fig. 4.

The influence of convection on surface wind anomalies is illustrated in a schematic (Fig. 10). This shows both the convergence feedback discussed in 4.2 and the effect of vertical momentum transport discussed here.

Our results suggest that surface wind anomalies are strong when the underlying SSTs are warm, and weak when the underlying SSTs are cool. This is reminiscent of the wind-SST relation observed in regions of strong SST fronts (Wallace et al. 1989; Chelton et al. 2001; Xie 2004a; Small et al. 2008), where surface winds accelerate when they encounter warmer SSTs. Various explanations for this behavior have been put forward (see Small et al. 2008 for a review), one of them being the enhanced vertical mixing of momentum inside the ABL that results when surface heat fluxes destabilize the ABL from below. It is not clear to what extent this mechanism applies to the western equatorial Atlantic. The meridional SST gradient is relatively weak there (see Fig. 1) and so is the correlation of SST and surface wind speed (Fig. 1 of Small et al. 2008). Moreover, the phenomenon is mostly observed for short temporal (sub-seasonal) and small spatial (< 1000 km) scales, which are different from the scales at hand (interannual; 2000 km or larger). Further analysis will be needed to clarify the link between the two phenomena and the mechanisms involved.

5. Comparison with the tropical Pacific and Indian Oceans

Seasonal migration of the ITCZ is common to all three tropical ocean basins. If the collocation of wind variability with the ITCZ position is a general feature of the tropics, rather than a peculiarity of the tropical Atlantic, then we would expect significant modulation of the equatorial modes of interannual variability in the other two basins as well. For the Pacific, several studies have already suggested an important role of the ITCZ in the phase locking of ENSO, though alternative hypotheses involving oceanic processes have been put forward (e.g. Schopf and Suarez 1988; Picaut et

al. 1997; Jin 1997; Weisberg and Wang 1997). The Indian Ocean also hosts an equatorial mode of variability usually referred to as the Indian Ocean Dipole (IOD; Saji et al. 1999, Webster et al. 1999) that peaks in boreal fall. Positive IOD events are marked by anomalous warming in the western equatorial Indian Ocean and cooling in the eastern equatorial Indian Ocean and along the coast of Sumatra, which constitutes a weakening of the climatological zonal SST gradient.

We composite observations of full precipitation and surface zonal wind anomalies for positive AZM, El Niño, and positive IOD events and plot their seasonal evolution in latitude-time sections (Fig. 11). For AZM events (Fig. 11a; precipitation and surface zonal wind anomalies averaged from 40-10°W, SST anomalies averaged from 20°W-0) we see the familiar northward shift of surface wind anomalies that accompanies the northward migration of the ITCZ from April to August. The equatorial SST anomalies peak in June when the ITCZ has already shifted northward. In the case of Pacific Niños (Fig. 11b; precipitation and wind averaged from 160°E to 170°W, SST from 150-90°W) wind anomalies on the equator increase from July through October and this is accompanied by an increase in total precipitation on the equator, though maximum precipitation occurs off the equator at approximately 10°S and 8°N. The southern precipitation maximum is associated with the South Pacific Convergence Zone (SPCZ), a perennial feature of the tropical Pacific that is most active in boreal winter. With the intensification of the SPCZ, the zonal wind anomalies also intensify but shift south of the equator, which leads to decreased anomalies on the equator. The maximum SST anomalies in the eastern equatorial Pacific occur during December, when wind anomalies over the central Pacific are in decline. Note that, as in the case of the AZM (Figs. 3, 5 and 11a), wind anomalies remain westerly as they shift away from the equator. Maximum wind anomalies of about 4 m/s occur at 5°S in January, while on the equator wind anomalies have decreased by more than 1 m/s compared to their peak in October. Vecchi (2006) shows that qualitatively similar changes in the wind field during the 1997/98 El Niño were sufficient to bring about the termination of the event and McGregor et al. (2012) obtain similar results for a reduced-gravity ocean model with idealized wind forcing.

The composite positive IOD event shows the least compelling evidence for the role of ITCZ migration in influencing equatorial wind variability (Fig. 11c; precipitation and wind averaged from 70-100°E, SST from 90-100°E). Even here though, one can see a strengthening of easterly wind anomalies on the equator that coincides with

the intensification of precipitation from July through October just north of the equator. The eastern Indian Ocean SST anomalies peak in October and are located a few degrees south of the equator. Maximum wind anomalies shift southward from November onward as they follow the seasonal migration of the ITCZ. The situation in the Indian Ocean is further complicated by the remote influence of ENSO on surface winds, which becomes dominant in November, when the IOD starts decaying. The decrease of SST anomalies in the eastern pole of the IOD (not shown), on the other hand, is strongly related to the seasonal reversal of the winds along the shore of Sumatra (Li et al. 2003).

Comparison of the three composites suggests that the meridional extent of both the ITCZ and surface wind anomalies is narrowest in the tropical Atlantic. This likely explains the rapid decay of surface wind anomalies in the equatorial Atlantic as the ITCZ migrates northward. In the tropical western Pacific and Indian Ocean, on the other hand, deep convection over the equator is essentially active year round, so the shift of maximum precipitation away from the equator elicits a less drastic response in the surface wind anomalies.

Another difference between the Atlantic and the other basins is that in the former it is northward migration of the ITCZ that leads to event termination while in the latter it is southward migration. The different migration tendencies of the ITCZ are due to the different times of year during which events peak. While the AZM peaks in boreal summer, the IOD and ENSO peak in boreal fall and winter, respectively, when southern hemisphere warming leads to the southward migration of the ITCZ. Such a southward migration of the ITCZ does not have a counterpart in the Atlantic, partly because the South Atlantic convergence zone is well separated from the equatorial branch. In the Pacific, on the other hand, the South Pacific convergence zone is relatively close to the equator so that maximum precipitation shifts to about 10°S in boreal winter, while the Indian Ocean features significant precipitation north and south of the equator throughout the year with weak seasonality.

6. Summary and discussion

6.1. Summary

We have investigated the reasons for the seasonal phase locking of equatorial Atlantic SST variability, also known as the Atlantic zonal mode (AZM) or Atlantic Niño, using observations and GCM simulations and focusing on the role of surface winds.

Previous results indicate that the AZM is closely linked to the occurrence of wind variability over the western equatorial Atlantic, which peaks about one month before the AZM (e.g. Richter et al. 2014a). Given the close relation between surface wind anomalies and the AZM, any process controlling the seasonality of wind anomalies will also control the seasonality of the AZM. We have shown that the seasonal migration of the ITCZ fulfills this role because maximum wind anomalies invariably occur in vicinity to the ITCZ. Thus, as the ITCZ moves north of the equator in June, so do the zonal wind anomalies, leading to decaying wind anomalies on the equator and the eventual termination of the AZM in the following months. This mechanism applies to both positive and negative AZM events.

Several factors contribute to the association of the ITCZ with surface wind anomalies on the equator. 1) Total surface winds are weak in the ITCZ region and thus the retarding effect of zonal advection is weak. 2) The low total wind speed also leads to relatively low surface drag via the bulk relationship, and therefore less momentum is lost to the ocean. 3) Vertical momentum transport associated with the ITCZ either reduces the retarding effect of momentum entrainment from the free troposphere or mixes momentum anomalies into the ABL.

The above arguments explain why the ITCZ is closely associated with surface wind variability. The crucial variable for AZM phase locking, however, is the surface stress because it determines the dynamic forcing of the ocean. Only factors 1) and 3) are relevant for the rapid decay of wind stress anomalies in June and July. Factor 2), on the other hand, slows the decay because it increases the portion of momentum injected into the ocean.

The close correspondence of the ITCZ and equatorial wind variability that is prominent in the Atlantic basin also appears in the Pacific and Indian Oceans, as illustrated by Fig. 11. Vecchi (2006) and McGregor et al. (2012) pointed out the importance of ITCZ migration for El Niño termination. Their mechanism, however, relies on the total wind speed altering surface friction and Ekman convergence. In contrast, the present study argues for the importance of horizontal advection and vertical momentum transport, while wind speed changes only play a role in the decay of surface winds, not that of wind stress. Further study will be needed to clarify whether phase locking in the tropical Pacific and Atlantic relies on different mechanisms.

6.2. Discussion

One intriguing result of our analysis is that surface zonal wind anomalies in boreal summer decrease despite the surface zonal pressure gradient reaching its peak during this season. This indicates that a simple Lindzen-Nigam type model would overestimate the surface wind response to SST anomalies in the equatorial Atlantic. Non-linear terms like horizontal advection and vertical momentum transport are crucial to understand the actual behavior of surface winds. Detailed observational studies of vertical momentum transport will be necessary to fully understand the roles of individual processes such as ABL entrainment and convective momentum transport.

Our results also indicate that the convergence feedback is not the main driver for enhanced surface wind anomalies under deep convection, though it plays some role. This suggests that the parameterization of the convergence feedback in intermediate complexity models, such as the Zebiak-Cane model (Zebiak and Cane 1987), should be reinterpreted if not reformulated.

We have seen that the peak in thermocline deepening and SST warming lags the peak in surface wind anomalies by one month. The delayed peak in SST is partly due to the time it takes Kelvin waves to communicate the signal to the east (Polo et al. 2008; Richter et al. 2014a). Due to the small Atlantic basin size, however, this delay may be rather short. Polo et al. (2008) estimate the Kelvin phase speed to range from 1.5 to 2.1 m/s. Assuming the waves originate from the center of the WEA region (30°W) and travel to the center of the ATL3 region (10°W), the delay would be 12-17 days. More detailed analysis will be needed to clarify the role of wave propagation.

An additional factor in AZM phase locking is the seasonality of upwelling in the eastern equatorial Atlantic, which is related to the rapid intensification of equatorial easterlies in late boreal spring and early summer (section 3; Richter et al. 2014a). The intensification, in turn, is related to the northward shift of the ITCZ during the same period, which leads to strong cross equatorial flow from a southeasterly direction (Fig. 1). The seasonal intensification of upwelling, shoals the mean thermocline, brings Kelvin-wave induced subsurface temperature anomalies to the surface and maximizes the surface expression of the event (Okumura and Xie 2006). Thus our results suggest that the northward migration of the ITCZ in late spring/early summer controls the seasonality of the AZM in two ways: 1) The associated cross-equatorial northeasterly flow leads to a strengthening of the full-field equatorial easterlies and upwelling. This

brings ocean temperature anomalies to the surface and maximizes SST anomalies. 2) Surface wind anomalies shift north of the equator thus ushering in the demise of the AZM event. This is in line with the sensitivity studies of Bates (2008, 2010).

Our results suggest that the spring peak of wind anomalies on the equator is due to the proximity of the ITCZ. This, in turn, is associated with maximum solar insolation and surface temperatures being centered on the equator during spring. The reason why the ITCZ attains this position only once per year has been attributed to various causes, such as the alignment of coast and surface wind leading to interhemispheric differences in upwelling-related cooling (Philander et al. 1996; Xie 2004b), or the interhemispheric temperature gradient induced by the Atlantic meridional overturning circulation (Frierson and Hwang 2012; Fuckar et al. 2013; Marshall et al. 2014). Regardless of the underlying causes for this ITCZ behavior, its consequences for AZM phase locking are evident.

Previous studies suggest that the ITCZ latitude is sensitive to subtropical and extratropical SST anomalies (Frierson and Hwang 2012; Fuckar et al. 2013). We have shown that the ITCZ position strongly modulates equatorial Atlantic variability. Taken together, these two facts hint at the possibility of remote influences on equatorial Atlantic variability. Furthermore, past and future mean state SST changes may profoundly influence the AZM via changes in ITCZ behavior. If, e.g., the ITCZ were to stay north of the equator throughout the year, it would greatly reduce wind and SST variability on the equator. Thus the results of the present study provide a new angle from which to examine climate change impacts in the Atlantic basin.

Acknowledgments

The authors thank Noel Keenlyside and Tim Li for helpful discussions. The two anonymous reviewers are thanked for their constructive comments that helped improve the manuscript.

References

- Adler RF, Huffman GJ, Chang A, Ferraro R, Xie P, Janowiak J, Rudolf B, Schneider U, Curtis S, Bolvin D, Gruber A, Susskind J, Arkin P (2003) The Version 2 Global Precipitation Climatology Project (GPCP) Monthly Precipitation Analysis (1979-Present). *J Hydrometeor* 4:1147-1167
- Balmaseda MA, Mogensen K, Weaver AT (2013), Evaluation of the ECMWF ocean reanalysis system ORAS4. *QJR Meteorol Soc* 139:1132–1161. doi: 10.1002/qj.2063
- Bates SC (2008) Coupled ocean–atmosphere interaction and variability in the tropical Atlantic Ocean with and without an annual cycle. *J Clim* 21:5501–5523
- Bates, SC (2010) Seasonal influences on coupled ocean–atmosphere variability in the tropical Atlantic Ocean. *J Clim* 23:582–604
- Biasutti M, Battisti DS, Sarachik ES (2003) The annual cycle over the Tropical Atlantic, South America, and Africa. *J Clim* 16:2491–2508
- Biasutti M, Battisti DS, Sarachik ES (2005) Terrestrial influence on the annual cycle of the Atlantic ITCZ. *J Clim* 18:211–228
- Bjerknes J (1969) Atmospheric teleconnections from the equatorial Pacific. *Mon Weather Rev* 97:163-172
- Breugem WP, Hazeleger W, Haarsma RJ (2006) Multimodel study of tropical Atlantic variability and change. *Geophys Res Lett* 33. doi:10.1029/2006GL027831
- Carton JA, Huang B (1994) Warm events in the tropical Atlantic. *J Phys Oceanogr* 24:888–903
- Chang P, Coauthors (2006) Climate Fluctuations of Tropical Coupled Systems—The Role of Ocean Dynamics. *J Clim* 19:5122–5174
- Chelton DB, Esbensen SK, Schlax MG, Thum N, Freilich MH, Wentz FJ, Gentemann CL, McPhaden MJ, Schopf PS (2001) Observations of coupling between surface wind stress and sea surface temperature in the Eastern Tropical Pacific. *J Clim* 14:1479-1498
- Davey MK, Coauthors (2002) STOIC: a study of coupled model climatology and variability in tropical ocean regions. *Clim Dyn* 18:403-420
- Dee DP, Coauthors (2011) The ERA-Interim reanalysis: configuration and performance of the data assimilation system. *Quart J R Meteorol Soc* 137:553-597
- Ding H, Keenlyside NS, Latif M (2010) Equatorial Atlantic interannual variability: the role of heat content. *J Geophys Res* 115. doi:10.1029/2010JC006304
- Folland CK, Palmer TN, Parker DE (1986) Sahel rainfall and world-wide sea temperatures. *Nature* 320:602-607
- Foltz GR, McPhaden MJ (2010) Abrupt equatorial wave-induced cooling of the Atlantic cold tongue in 2009. *Geophys Res Lett* 37, L24605, doi:10.1029/2010GL045522.
- Frierson DMW, Hwang Y-T (2012) Extratropical influence on ITCZ shifts in slab ocean simulations of global warming. *J Clim* 25:720-733
- Fuckar NS, Xie S-P, Farneti R, Maroon E, Frierson DMW (2013). Influence of the extratropical ocean circulation on the intertropical convergence zone in an idealized coupled general circulation model. *J Clim* 26:4612-4629
- Gill AE (1980) Some simple solutions for heat-induced tropical circulation. *Q J R Meteorol Soc* 106:447–462

- Harrison DE, Vecchi GA (1999) On the termination of El Niño. *Geophys Res Lett* 26:1593–1596
- Huang B, Schopf PS, Shukla J (2004) Intrinsic Ocean-Atmosphere variability of the tropical Atlantic Ocean. *J Clim* 17:2058–2077
- Huang B, Shukla J (2005) Ocean–atmosphere interactions in the tropical and subtropical Atlantic Ocean. *J Clim* 18:1652–1672
- Jin F (1997) An equatorial ocean recharge paradigm for ENSO. Part I: Conceptual model. *J Atmos Sci* 54:811–829
- Keenlyside NS, Latif M (2007) Understanding equatorial Atlantic interannual variability. *J Clim* 20:131–142
- Li T, Wang B, Chang C-P, Zhang Y (2003) A theory for the Indian Ocean dipole-zonal mode. *J Atmos Sci* 60:2119–2135
- Lindzen RS, Nigam S (1987) On the role of the sea surface temperature gradients in forcing the low-level winds and convergence in the tropics. *J Atmos Sci* 44:2418–2436
- Lübbecke JF, Böning CW, Keenlyside NS, Xie S-P (2010) On the connection between Benguela and equatorial Atlantic Niños and the role of the South Atlantic Anticyclone. *J Geophys Res* 115(C9):C09015. doi: 10.1029/2009JC005964
- Lübbecke JF, McPhaden MJ (2012) On the Inconsistent Relationship between Pacific and Atlantic Niños. *J Climate* 25:4294–4303
- Marshall J, Donohoe A, Ferreira D, McGee D (2014) The ocean’s role in setting the mean position of the inter-tropical convergence zone. *Clim Dyn* 42:1967–1979
- Matsuno T (1966) Quasigeostrophic motions in the equatorial area. *J Meteor Soc Japan* 44:25–43.
- McGregor S, Timmermann A, Schneider N, Stuecker MF, England MH (2012) The effect of the South Pacific Convergence Zone on the termination of El Niño events and the meridional asymmetry of ENSO. *J Climate* 25:5566–5586
- Neelin, JD, Battisti DS, Hirst AC, Jin F-F, Wakata Y, Yamagata T, Zebiak S (1998) ENSO Theory. *J Geophys Res* 103:14261–14290
- Nobre P, Shukla J (1996) Variations of sea surface temperature, wind stress, and rainfall over the tropical Atlantic and South America. *J Clim* 9:2464–2479
- Okumura Y, Xie S-P (2004) Interaction of the Atlantic equatorial cold tongue and African monsoon. *J Clim* 17:3588–3601
- Philander SGH (1986) Unusual conditions in the tropical Atlantic Ocean in 1984. *Nature* 322:236–238
- Philander SGH, Gu D, Halpern D, Lambert G, Lau NC, Li T, Pacanowski RC (1996) Why the ITCZ is mostly north of the equator. *J Climate* 9:2958–2972
- Picaut J, Masia F, du Penhoat Y (1997) An advective-reflective conceptual model for the oscillatory nature of the ENSO. *Science* 277:663–666
- Polo I, Lazar A, Rodriguez-Fonseca B, Arnault S (2008) Oceanic Kelvin waves and tropical Atlantic intraseasonal variability: 1. Kelvin wave characterization. *J Geophys Res* 113(C07009). doi:10.1029/2007JC004495
- Reynolds RW, Rayner NA, Smith TM, Stokes DC, Wang W (2002) An improved in situ and satellite SST analysis for climate. *J Clim* 15:1609–1625
- Richter I, Xie S-P (2008) On the origin of equatorial Atlantic biases in coupled general circulation models. *Clim Dyn* 31:587–598
- Richter I, Behera SK, Masumoto Y, Taguchi B, Komori N, Yamagata T (2010) On the triggering of Benguela Niños: remote equatorial versus local influences. *Geophys Res Lett* 37:L20604. doi:10.1029/2010GL044461

- Richter I, Behera SK, Masumoto Y, Taguchi B, Sasaki H, Yamagata T (2013) Multiple causes of interannual sea surface temperature variability in the equatorial Atlantic Ocean. *Nature Geosci* 6:43-47
- Richter I, Xie S-P, Behera SK, Doi T, Masumoto Y (2014a) Equatorial Atlantic variability and its relation to mean state biases in CMIP5. *Clim Dyn* 42:171-188, doi: 10.1007/s00382-012-1624-5
- Richter I, Behera SK, Doi T, Taguchi B, Masumoto Y, Xie, S-P (2014b) What controls equatorial Atlantic winds in boreal spring? *Clim Dyn* 43:3091–3104.
- Saji HN, Goswami BN, Vinayachandran PN, Yamagata T (1999) A dipole mode in the tropical Indian Ocean. *Nature* 401:360–363
- Schopf PS, Suarez MJ (1988) Vacillations in a coupled ocean–atmosphere model. *J Atmos Sci* 45:549–566
- Small RJ, deSzoeke SP, Xie S-P, O’Neill L, Seo H, Song Q, Cornillon P, Spall M, Minobe S (2008) Air-sea interaction over ocean fronts and eddies. *Dyn Atmospheres Oceans* 45:274-319
- Stockdale TN, Balmaseda MA, Vidard A (2006) Tropical Atlantic SST prediction with coupled ocean-atmosphere GCMs. *J Clim* 19:6047-6061
- Vecchi GA (2006) The termination of the 1997–98 El Niño. Part II: mechanisms of atmospheric change. *J Clim* 19:2647–2664. doi: 10.1175/JCLI3780.1
- Wallace JM, Mitchell TP, Deser C (1989) The influence of sea surface temperature on surface wind in the eastern tropical Pacific: seasonal and interannual variability. *J Clim* 2: 1492-1499.
- Webster PJ (1981) Mechanisms determining the atmospheric response to large-scale sea surface temperature anomalies. *J Atmos Sci* 38:554-571
- Webster PJ, Moore A, Loschnigg J, Leban M (1999) Coupled ocean–atmosphere dynamics in the Indian Ocean during 1997–1998. *Nature* 401:356–360
- Weisberg RH, Wang C (1997) A western Pacific oscillator paradigm for the El Niño–Southern Oscillation. *Geophys Res Lett* 24:779–782
- Xie S-P (2004a) Satellite observations of cool ocean-atmosphere interaction. *Bull Amer Meteor Soc* 85:195-208
- Xie S-P (2004b) The shape of continents, air-sea interaction, and the rising branch of the Hadley circulation. In *The Hadley Circulation: Past, Present and Future*, H. F. Diaz and R. S. Bradley (eds.), Kluwer Academic Publishers, Dordrecht, 121-152
- Xie S-P, Carton JA (2004) Tropical Atlantic variability: Patterns, mechanisms, and impacts. In *Earth Climate: The Ocean-Atmosphere Interaction*, C. Wang, S.-P. Xie and J.A. Carton (eds.), Geophysical Monograph, 147, AGU, Washington D.C., 121-142.
- Zebiak SE (1986) Atmospheric convergence feedback in a simple model for El Niño. *Mon Wea Rev* 114:1263-1271
- Zebiak SE (1993) Air–sea interaction in the equatorial Atlantic region. *J Clim* 6:1567–1586
- Zebiak SE, Cane A (1987) A model El Niño–Southern oscillation. *Mon Weather Rev* 115:2262–2278

A. Tables

model	horizontal grid	# vertical levels
ACCESS1-0	1.875° x 1.25°	38
ACCESS1-3	1.875° x 1.25°	38
bcc-csm1-1	T42 (2.8°)	26
bcc-csm1-1-m	T42 (2.8°)	26
BNU-ESM	T42 (2.8°)	26
CanAM4	T63 (1.8°)	35
CCSM4	1.25° x 0.9°	26
CESM1-CAM5	1.25° x 0.9°	26
CMCC-CM	T159 (0.75°)	31
CNRM-CM5	T127 (1.5°)	31
CSIRO-Mk3-6-0	T63 (1.9°)	18
EC-EARTH	T159 (1.25°)	62
FGOALS-g2	2.8125° x 2.8125°	26
FGOALS-s2	R42 (2.8° x 1.7°)	26
GFDL-CM3	200 km (2°)	48
GFDL-HIRAM-C180	C180 (0.5°)	32
GFDL-HIRAM-C360	C360 (0.25°)	32
GISS-E2-R	2° x 2.5°	29
HadGEM2-A	1.875° x 1.25°	60
inmcm4	2° x 1.5°	21
IPSL-CM5A-LR	3.75° x 1.9°	39
IPSL-CM5A-MR	1.25° x 2.5°	39
IPSL-CM5B-LR	3.75° x 1.9°	39
MIROC5	T85 (1.4°)	40
MIROC-ESM	T42 (2.8°)	80
MPI-ESM-LR	T63 (1.8°)	47
MPI-ESM-MR	T63 (1.8°)	95
MRI-AGCM3-2H	T319 (60km)	64
MRI-AGCM3-2S	T959 (20km)	64
MRI-CGCM3	T159 (1.125°)	35
NorESM1-M	2.5° x 2.9°	26

Table 1. CMIP5 GCMs used for the amip ensemble average. Horizontal and vertical resolution are given in columns 2 and 3, respectively.

B. Figures

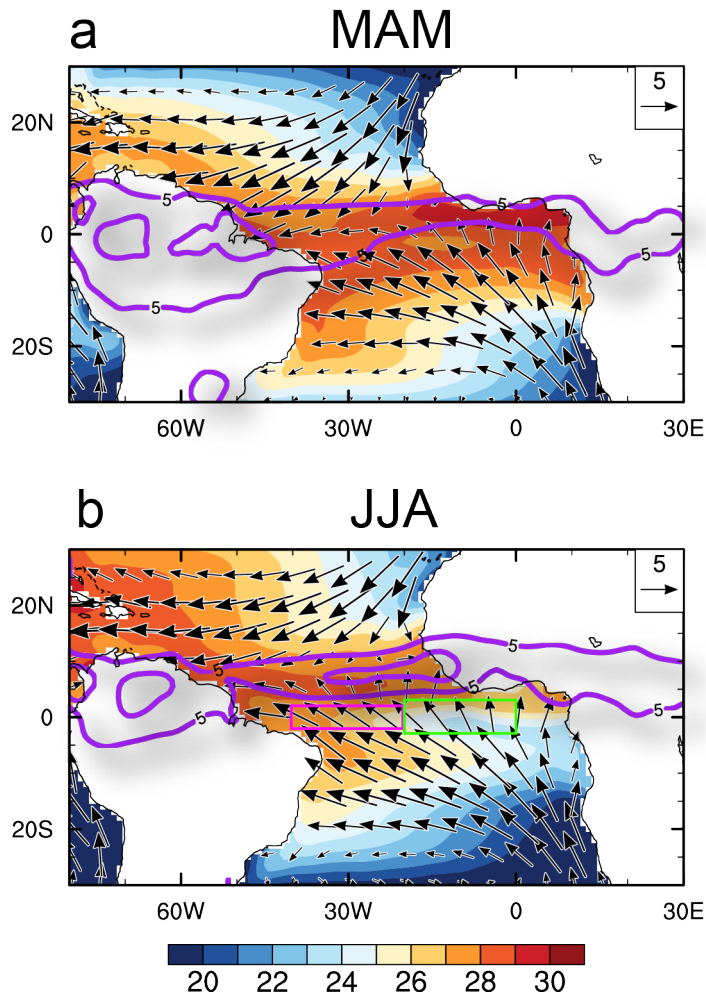


Figure 1. OI SST (shading; °C), ERAI surface winds (vectors; reference 5 m/s), and GPCP precipitation (5 and 10 mm/d contours) for a) MAM, and b) JJA. The two rectangles centered on the equator in panel b) show the WEA (left) and ATL3 (right) regions.

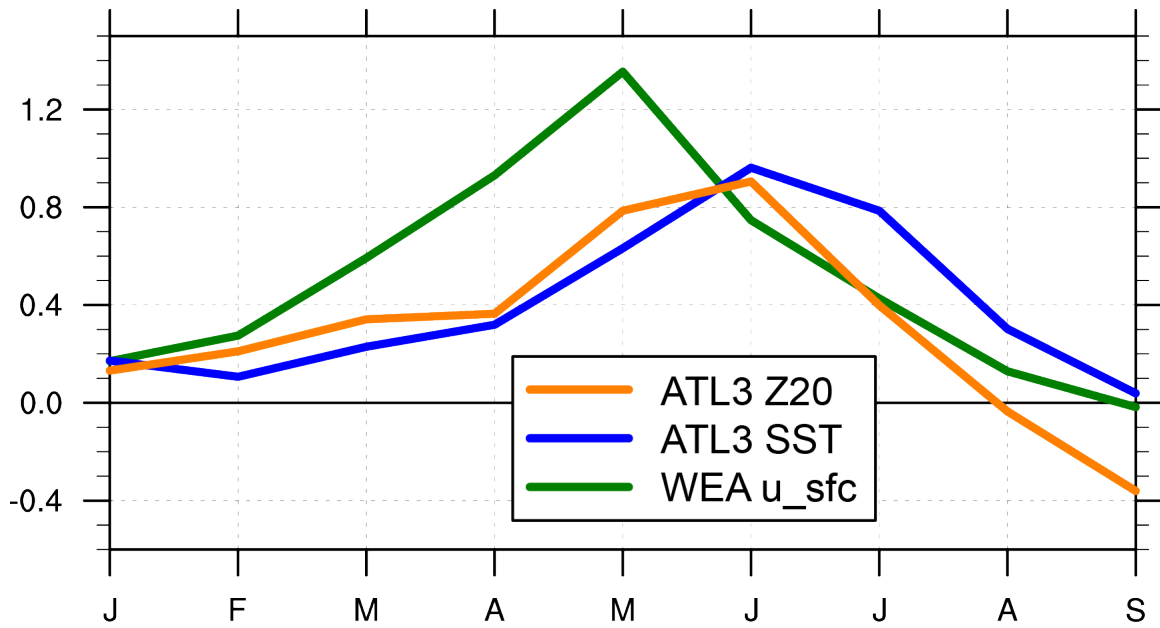


Figure 2. ERA-Interim atmospheric reanalysis WEA surface zonal wind anomaly (green line; m/s), ORAS-4 ocean reanalysis ATL3 SST anomaly (blue line; K), and ORAS-4 ocean reanalysis ATL3 20°C-isotherm anomaly (orange line; m*0.1). Fields are composited on positive AZM events (canonical Atlantic Niño).

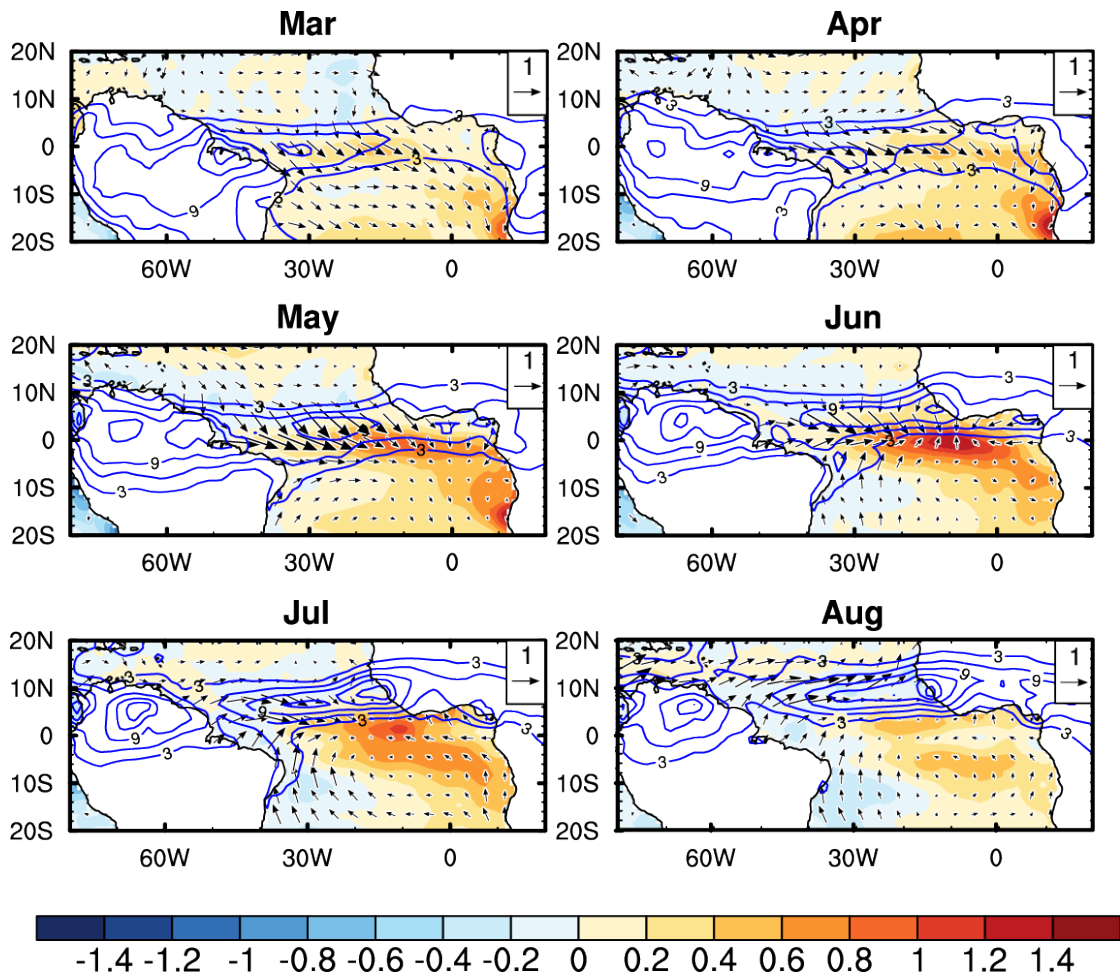


Figure 3. OI SST anomalies (shading; K), ERAI surface wind anomalies (vectors; reference 1 m/s), and total precipitation (contour lines; interval 3 mm/d) composited on positive AZM events (canonical Atlantic Niño).

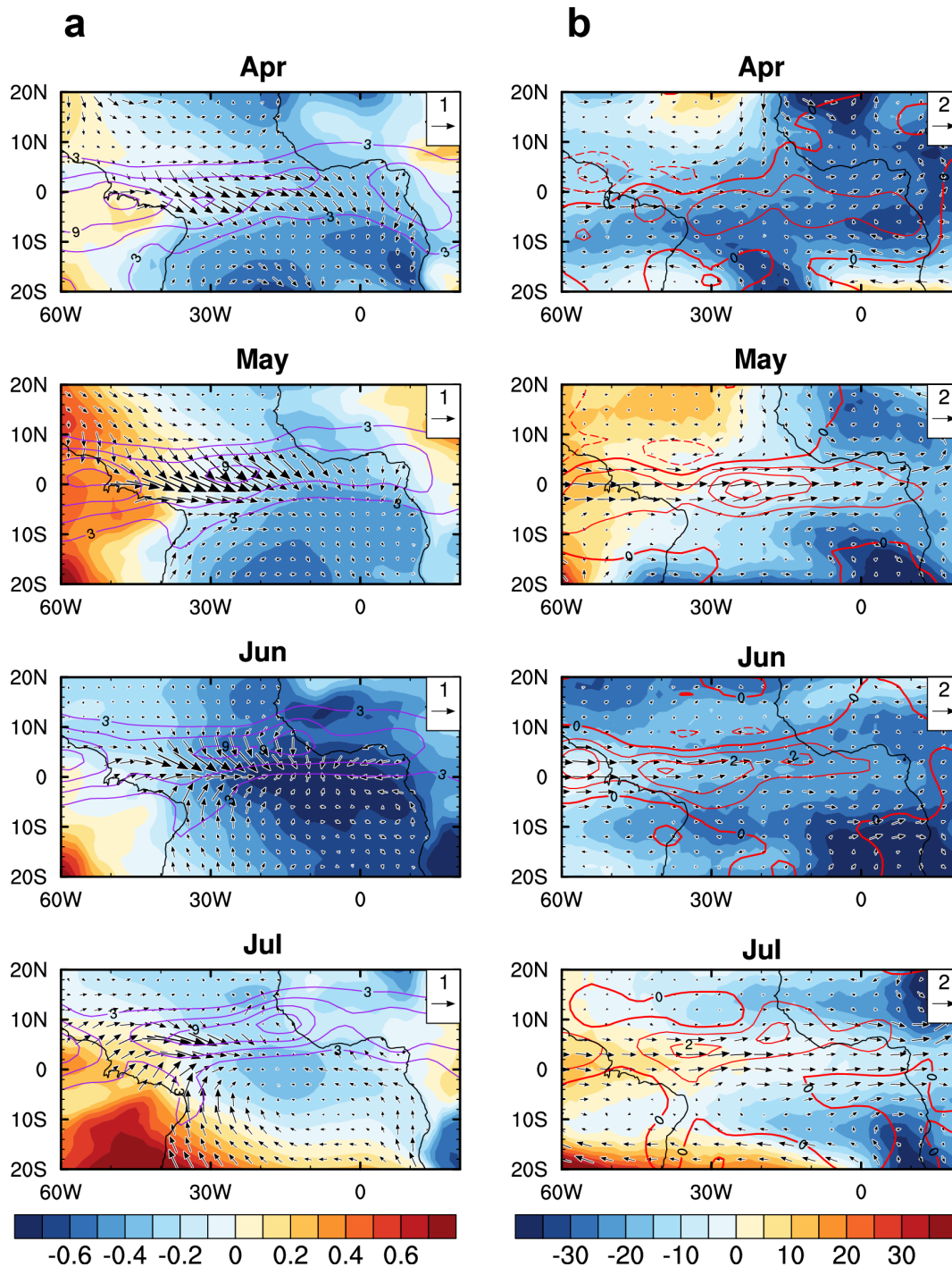


Figure 4. Observational and reanalysis fields composited on positive AZM events (canonical Atlantic Niños). a) Anomalous sea-level pressure (shading; hPa), anomalous surface winds (vectors; reference 1 m/s), and total precipitation (contours; interval 3 mm/d). b) Anomalous geopotential height at 700 hPa (shading; m), anomalous winds at 700 hPa (vectors; reference 2 m/s), and anomalous precipitation (red contours; interval 1 mm/day).

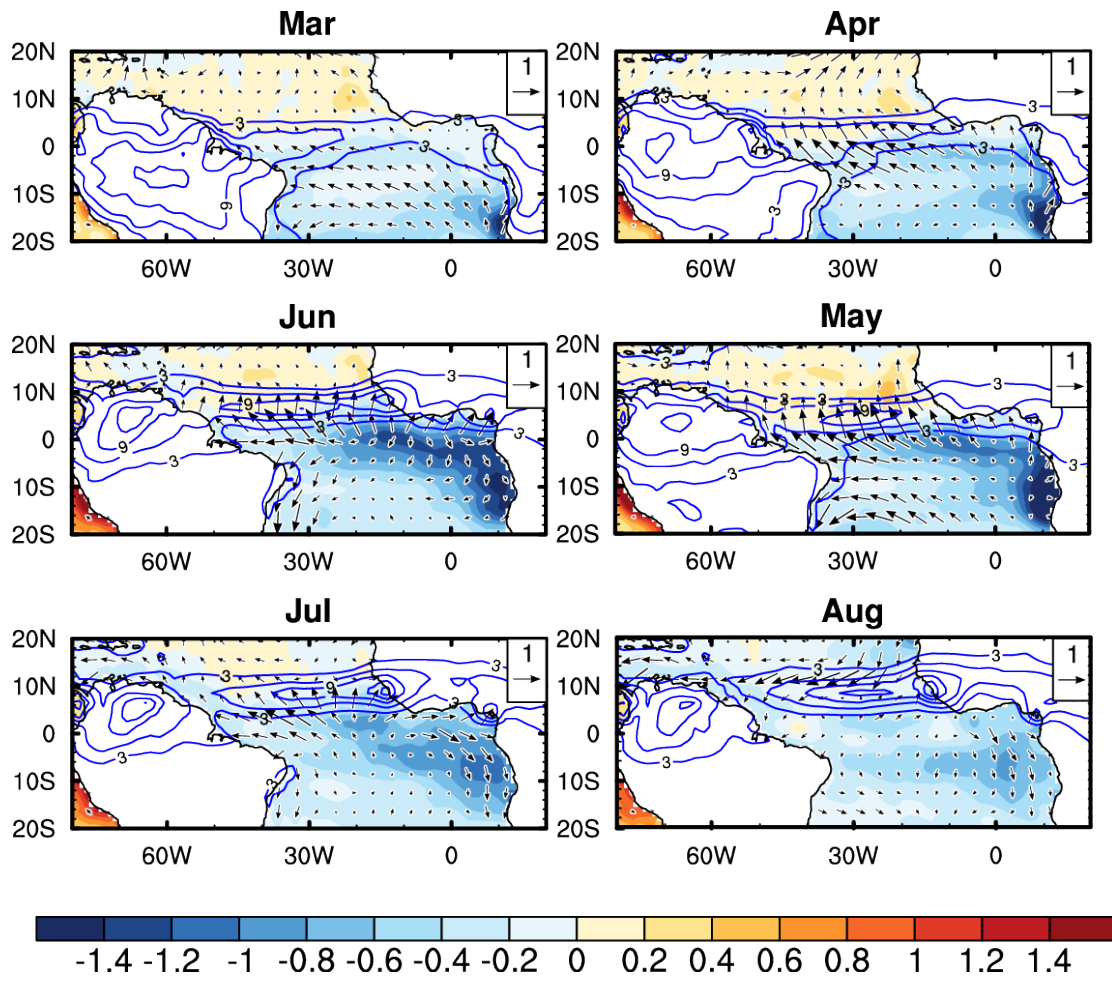


Figure 5. As in Fig. 3, but for fields composited on negative AZM events (canonical Atlantic Niña) years.

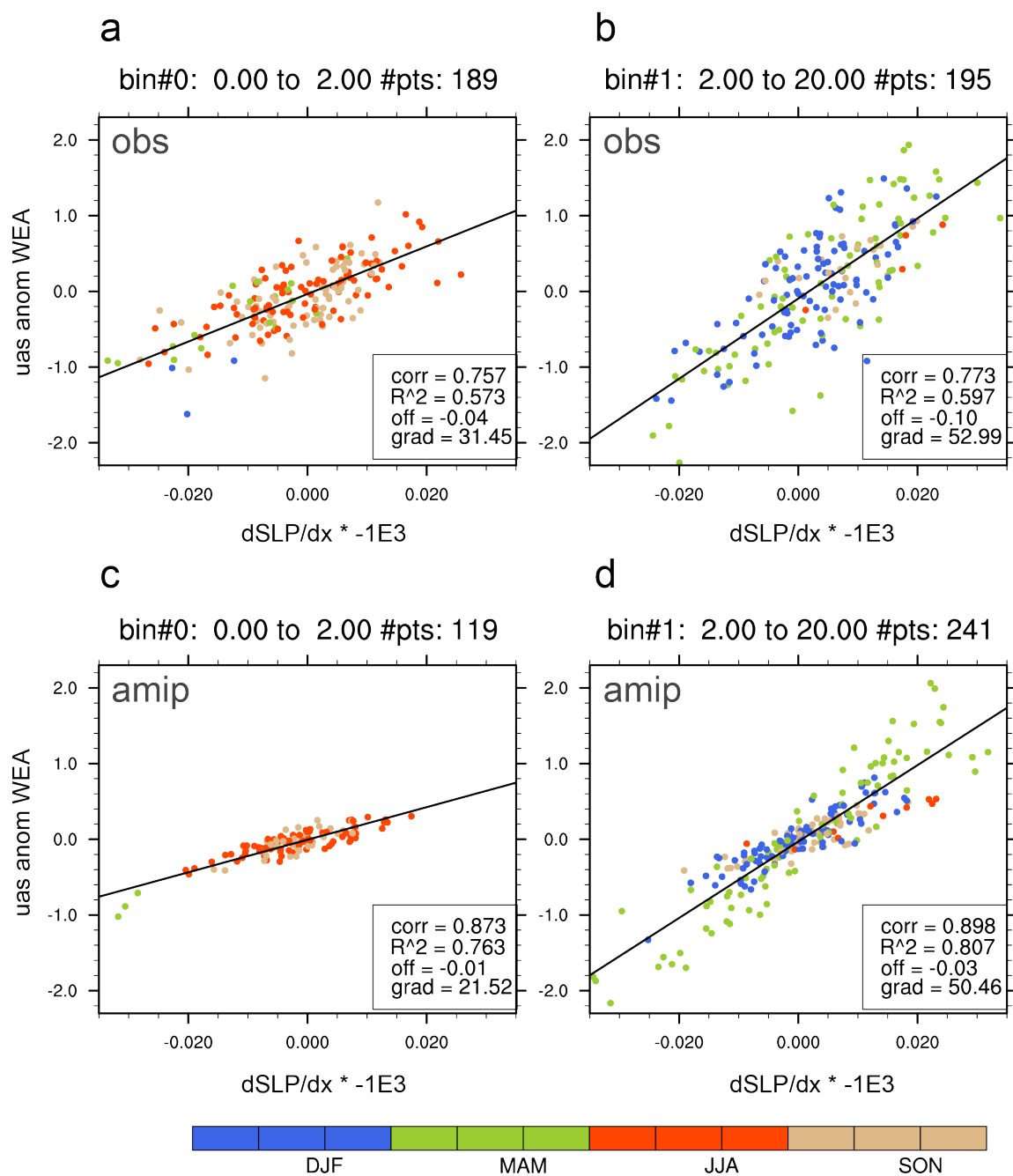


Figure 6. Scatter plots of WEA zonal wind anomalies (m/s) versus WEA pressure gradient anomalies ($\text{Pa/m} \cdot 10^3$) for observations (top row) and the AMIP ensemble (bottom row). The left column shows months for which WEA precipitation is below 2 mm/day, the right column months for which WEA precipitation is above 2 mm/day. Color coding indicates the season of each data point.

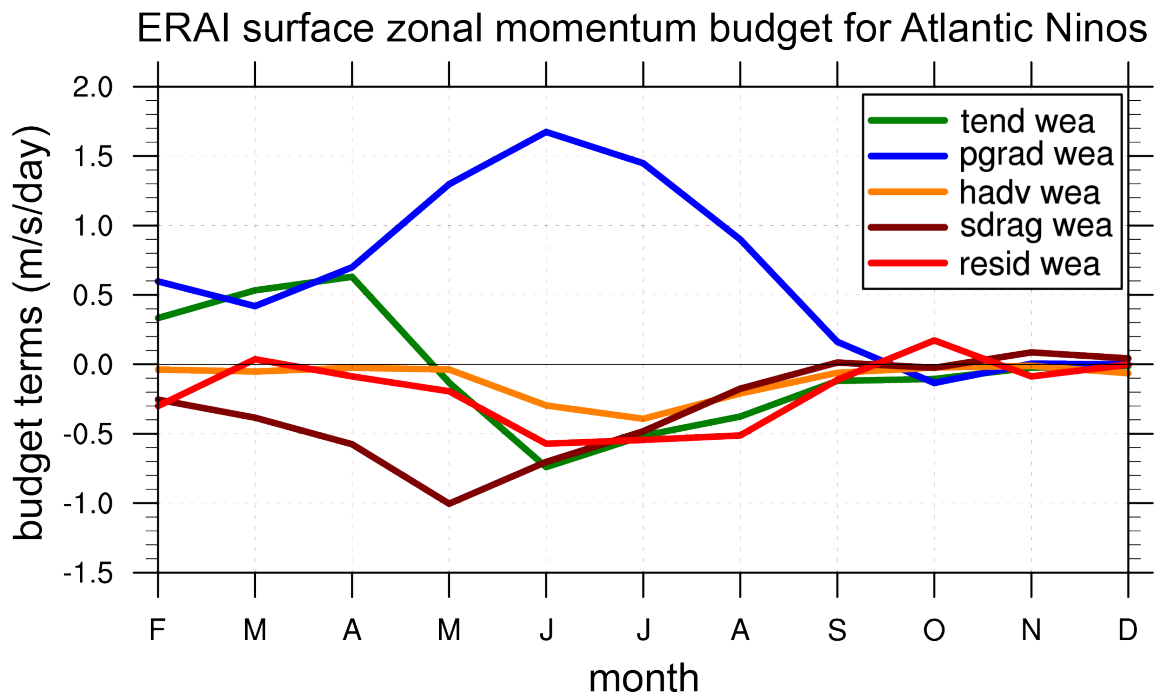


Figure 7. Composite evolution of terms in the surface zonal momentum budget calculated from ERA1 and averaged over the WEA region. Positive AZM events (canonical Atlantic Niños) are selected for the composite. The individual terms are: zonal momentum tendency (green line; $\text{m/s/day} \times 50.0$), pressure gradient term (blue line; m/s/day), horizontal advection (orange line, m/s/day), surface drag (brown line; m/s/day), and the residual (red line; $\text{m/s/day} \times -1$). The residual has been multiplied by -1 to show the term needed to close the budget.

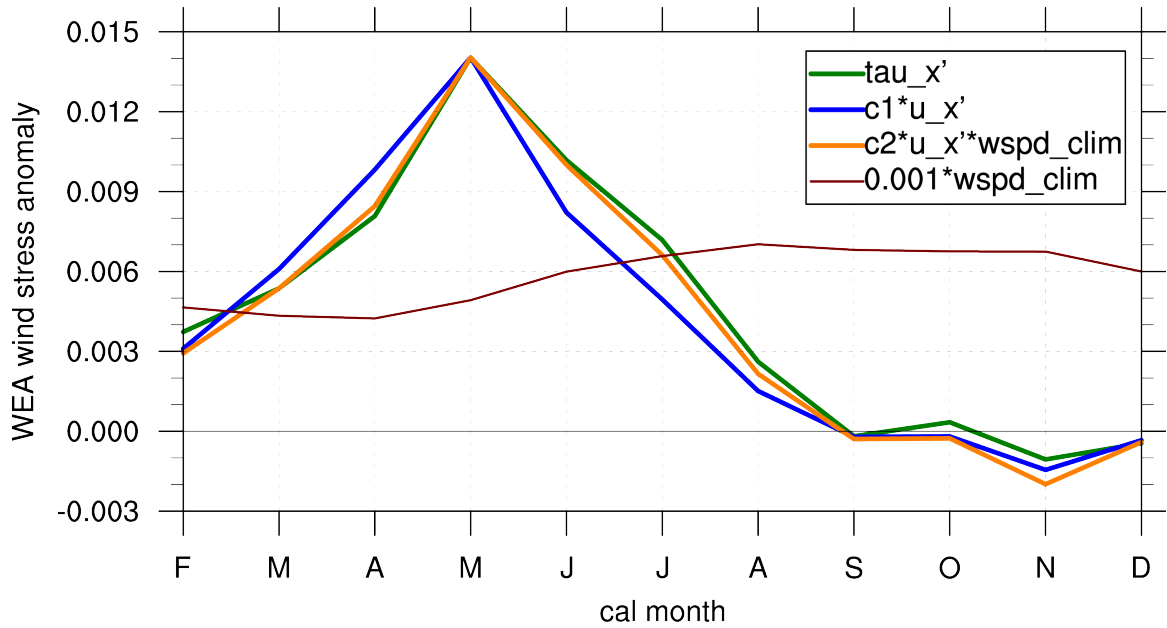


Figure 8. Composite evolution of surface wind related fields from the ERAI averaged over the WEA region. Positive AZM events (canonical Atlantic Niños) are selected for the composite. Four fields (units N m^{-2}) are shown: surface zonal wind stress anomaly (green line), surface zonal wind anomaly multiplied by a constant c_1 (blue line; $c_1=0.01 \text{ kg m}^{-2} \text{ s}^{-1}$), surface zonal wind anomaly multiplied by the climatological surface wind speed and a constant c_2 (orange line; $c_2=0.20 \text{ kg m}^{-3}$), and the climatological surface wind speed (brown line) multiplied by $0.001 \text{ kg m}^{-2} \text{ s}^{-1}$. The constants c_1 and c_2 are chosen such that the two derived fields have the same maximum as the zonal wind stress anomaly in May.

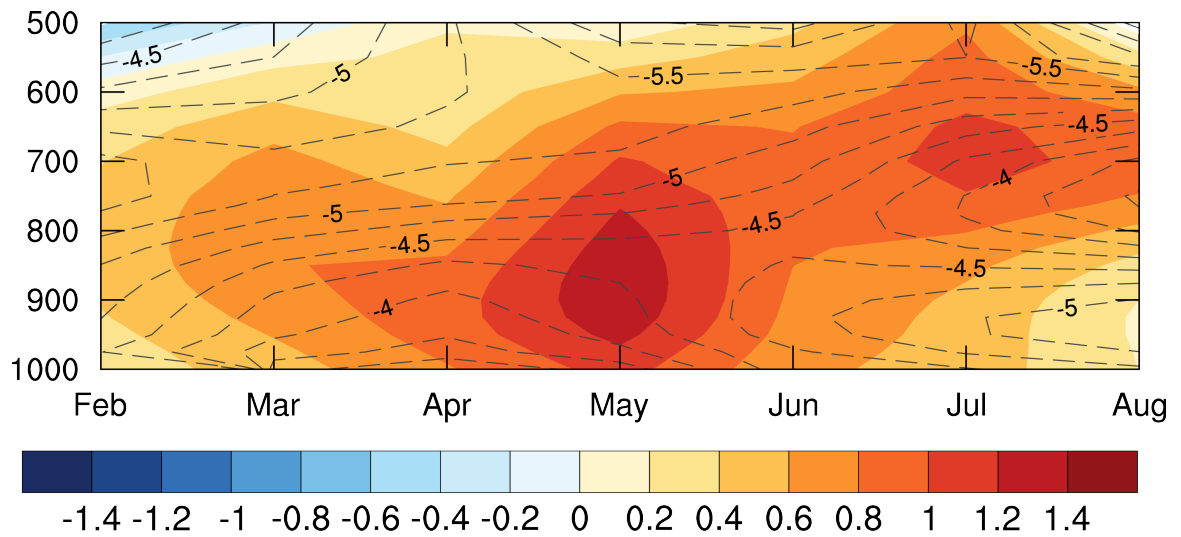


Figure 9. Time-pressure section of composited zonal wind anomaly (shading; m/s) and total zonal wind (contours; interval 0.25 m/s, averaged over the western equatorial Atlantic (WEA region) from ERAI data. Positive AZM events (canonical) Atlantic Niños are selected for the composites.

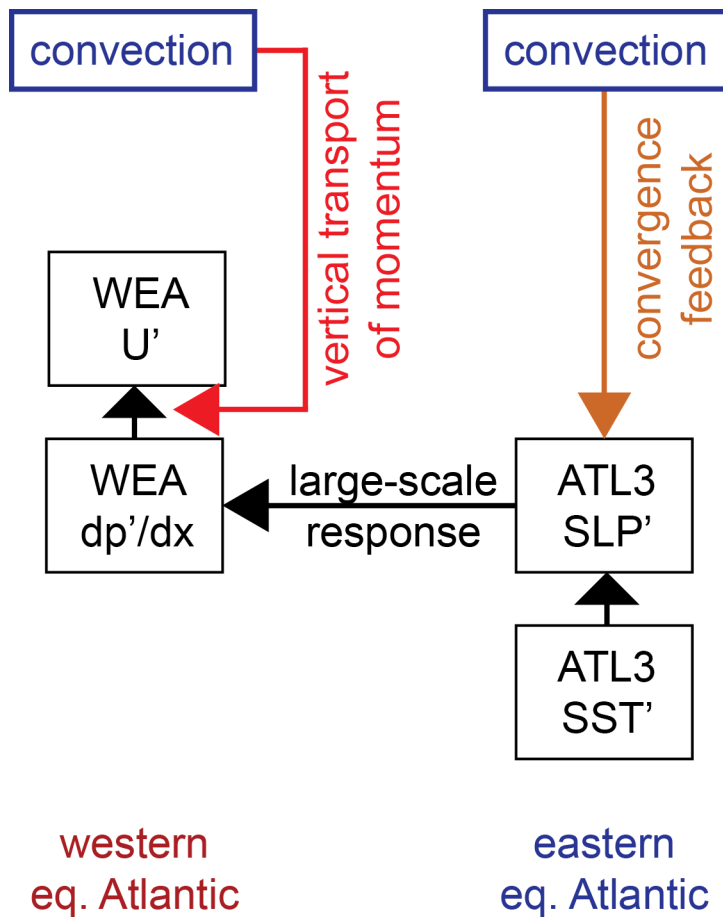


Figure 10. Schematic illustrating the influence of convergence feedback and vertical momentum transport. A warm SST anomaly in the ATL3 region reduces local sea-level pressure (SLP). If the SST anomaly is able to trigger deep convection, the SLP response will be enhanced through diabatic heating of the troposphere. Due to the large-scale response to convection anomalies the SLP anomalies extend to the west. This leads to an SLP gradient in the WEA region that drives westerly wind anomalies. The presents study suggests that the influence of the SLP gradient on winds is modulated by deep convection through vertical momentum transport.

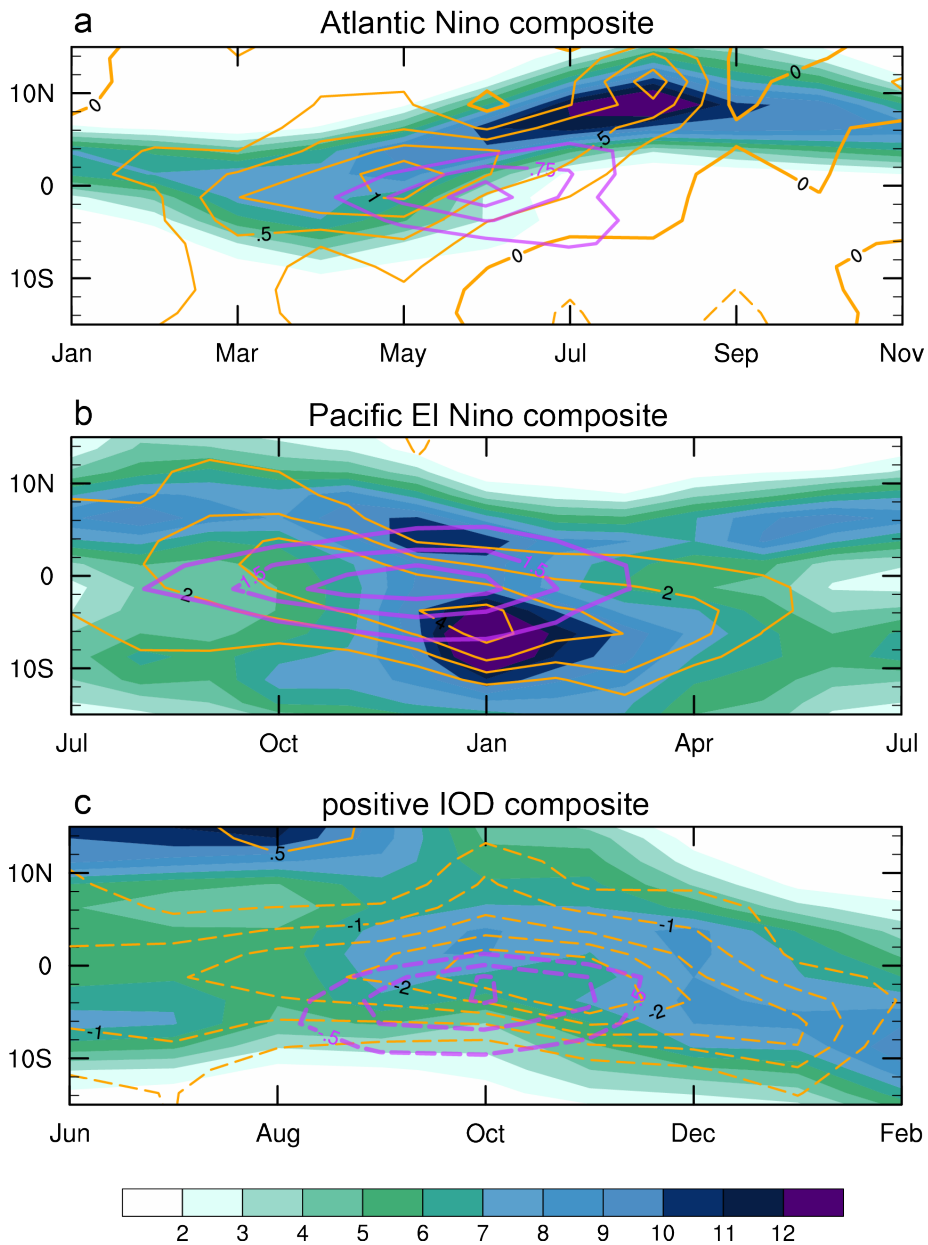


Figure 11. Latitude-time sections of GPCP full precipitation (shading; mm/day), ERAI surface zonal wind anomalies (yellow contours; m/s), and OI SST (purple contours; K) for composite a) positive AZM events (canonical Atlantic Niños) with precipitation and wind zonally averaged from 40-10°W and SST averaged from 20°W to 0, b) El Niños with precipitation and wind averaged from 160°E-170°W and SST averaged from 150 to 90°W, and c) positive IOD events with wind and precipitation averaged from 70-100°E, and SST averaged from 90 to 100°E. The contour interval for surface winds is 0.25 m/s for panel a, 1 m/s for panel b, and 0.5 m/s for panel c. The contour interval for SST is 0.25 K for panels a and c (contouring starts from 0.5 K and -0.5 K, respectively), and 0.5K for panel b (contouring starts from 1 K). Dashed lines indicate negative values.